Chemical-State Analysis of Li Compounds and Nitrogen-Getter Material for Liquid Li by Soft X-ray Emission Spectroscopy

AUTHOR(S):

Mukai, Keisuke; Omura, Ryo; Yagi, Juro; Kasada, Ryuta

Chemical-State Analysis of Li Compounds and Nitrogen-Getter Material for Liquid Li by Soft X-ray Emission Spectroscopy

Keisuke Mukai[1, 2], Ryo Omura[1], Juro Yagi[1], Ryuta Kasada[3]
[1] Institute of Advanced Energy, Kyoto University, [2] Kyoto Fusioneering Ltd. [3] Institute for Material Research, Tohoku University

Lithium metal and oxides are key compounds for Li air battery and nuclear fusion. Constructing two dimensional mappings is a useful approach to understand chemical behavior and degradation mechanism of such materials at the micro-scale. Herein, we employ the soft X-ray emission spectrometer (SXES) to analyze characteristic X-ray emission spectra from the Li metal/oxides and nitrogen-getter material immersed in liquid Li metal. The high energy resolutions allowed us to measure N–Kα and Ti–Lℓ emissions, separately. By comparing with the first-principle calculated density of states, the elemental and chemical state mappings in the degraded materials were successfully constructed.

Introduction

As light elements have attractive nuclear properties, low Z (Z: atomic number) materials are utilized as key components in nuclear fission and fusion. Such materials are used in an extreme condition, such as high temperature, chemically corrosive environments, and intense neutron flux. Thus, it is of particular importance to understand those chemical behaviors and clarify degradation mechanisms, experimentally. We here employ a soft X-ray emission spectrometer (SXES) attached to an electron probe micro-analyzer (EPMA), which covers a low energy range (50–210 eV) with ultra-high energy resolutions as good as 0.2 eV [1,2]. In our previous studies, we report chemical state analysis of the low Z compounds utilized in the nuclear sector, including Li–Pb eutectic alloy, Be intermetallics, and B_4C [3–6]. Herein, we introduce our recent studies: (i) electron structure analysis and chemical state mapping for Li metal and oxides [7], (ii) SXES peak analysis for clarifying N distribution within Fe–Ti alloy getter immersed in liquid Li metal [8].

SXES analysis on Li metal and oxides

Motivation

Li metal and oxides can serve as a tritium breeding material in nuclear fusion reactors, which converts kinetic energy of neutrons into heat and simultaneously produces fuel tritium by nuclear transmutation [9]. Additionally, Li–O_2 air battery has attracted significant attentions as alternative means of electrochemical storage where a Li metal anode is oxidized and releases Li^+ to form discharge products of Li_2O_2 at the cathode [9,10]. Generally, Li metal and oxides are chemically reactive in ambient atmosphere to form impurity phases and corrosion products that can degrade performance and raise safety concerns. Chemical phase analysis of Li-containing products can help our understandings of chemical reactions and degradations in such systems. Herein, the SXES developed by JEOL was employed to assess electronic states in Li, Li_2O_2, and Li_2O for the chemical-state analysis. The SXES spectra are directly compared with the partial density of states (PDOS) of Li using density functional theory (DFT) calculations. Due to large errors in band calculations in oxides by DFT, not only a conventional functional based on the generalized gradient approximation (GGA) but also a hybrid functional were used in this study.

Methods

Commercially available Li metal rod, Li_2O, and Li_2O_2 powders were procured and stored in a glove box filled with Ar gas. The powder samples were analyzed by a JXA-8500F field emission electron probe micro-analyzer (FE-EPMA) by JEOL equipped with SXES (SS-94000SXES by JEOL). The grating JS50XL was used for the analysis [1]. The measurement time and the acceleration voltages of the electron beam were 60 s and 2.0 kV, respectively. DFT calculations were performed using the Perdew–Burke-Ernzerhof (PBE) functional and hybrid HSE06 functional implemented in the Vienna ab initio simulation package (VASP) [10–14]. The electron configurations $1s^22s^1$, $2s^22p^4$ were used for the Li and O atoms, respectively. For a direct comparison between SXES

〉〉 Kyoto 611-0011, Japan | E-mail: k-mukai@iae.kyoto-u.ac.jp

spectrum and occupied states by PDOS, the energy of PDOS was referenced to the Li 1*s* band centroid, $E_{\text{Li-1}s}$. $E_{\text{Li-1}s}$ was calculated as follows;

$$E_{\text{Li-1}s} = \frac{\int_{-\infty}^{E_{\max}} E g_{\text{Li-1}s}(E)dE}{\int_{-\infty}^{E_{\max}} g_{\text{Li-1}s}(E)dE}$$

where $g_{\text{Li-1}s}(E)$ and $E_{\max}$ are the density of states of Li 1*s* orbitals at E and maximum energy of the Li 1*s* orbitals, respectively.

Results and Discussion

X-ray powder diffraction (XRD) was carried out using Co–Kα, which indicated the formation of LiOH impurity phase in both of the Li_2O_2 and Li_2O samples. Multi-phase Rietveld refinements using the XRD data was carried out, which quantified ~6.3 and ~11.7 w.t.% of LiOH (space group: P4/*nmm*) in the Li_2O_2 and Li_2O samples respectively. **Figure 1** shows the SXES spectra of the Li metal, Li_2O_2, and Li_2O samples. In the obtained spectra, n^{th} order peaks of Li–Kα (n = 1) and O–Kα (n = 3–10) were observed. Peaks of C–Kα (n = 2 and 3) were also observed. Taking the XRD results into account, the C peak could derive not from Li_2CO_3 formation but from a carbon conduction tape. The Li–K spectrum of Li metal showed an asymmetric Doniach–Šunjić line shape in the range of 52–54.5 eV (Fig. 1b). The Li–K peak intensities for Li_2O_2 and Li_2O were significantly lower than that of Li. Ionization to Li^+ (oxidation) causes numerous Li valence electrons to be lost, and results in

Fig. 1

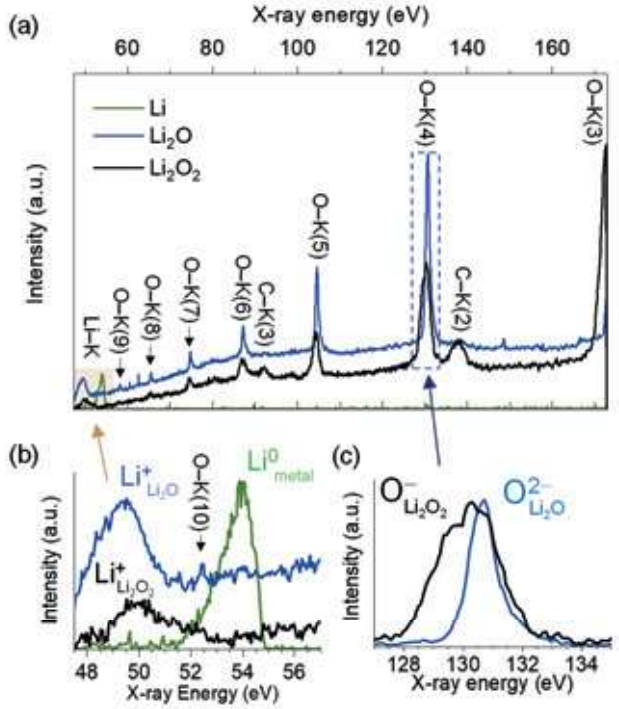

SXES spectra from the Li metal, Li_2O_2, and Li_2O samples in the energy ranges of 47.5–173 eV (a), 47.5–57 eV for Li–K (b), and 127–135 eV for O–K(4) (c), in which number in bracket denotes the X-ray diffraction order.

Fig. 2

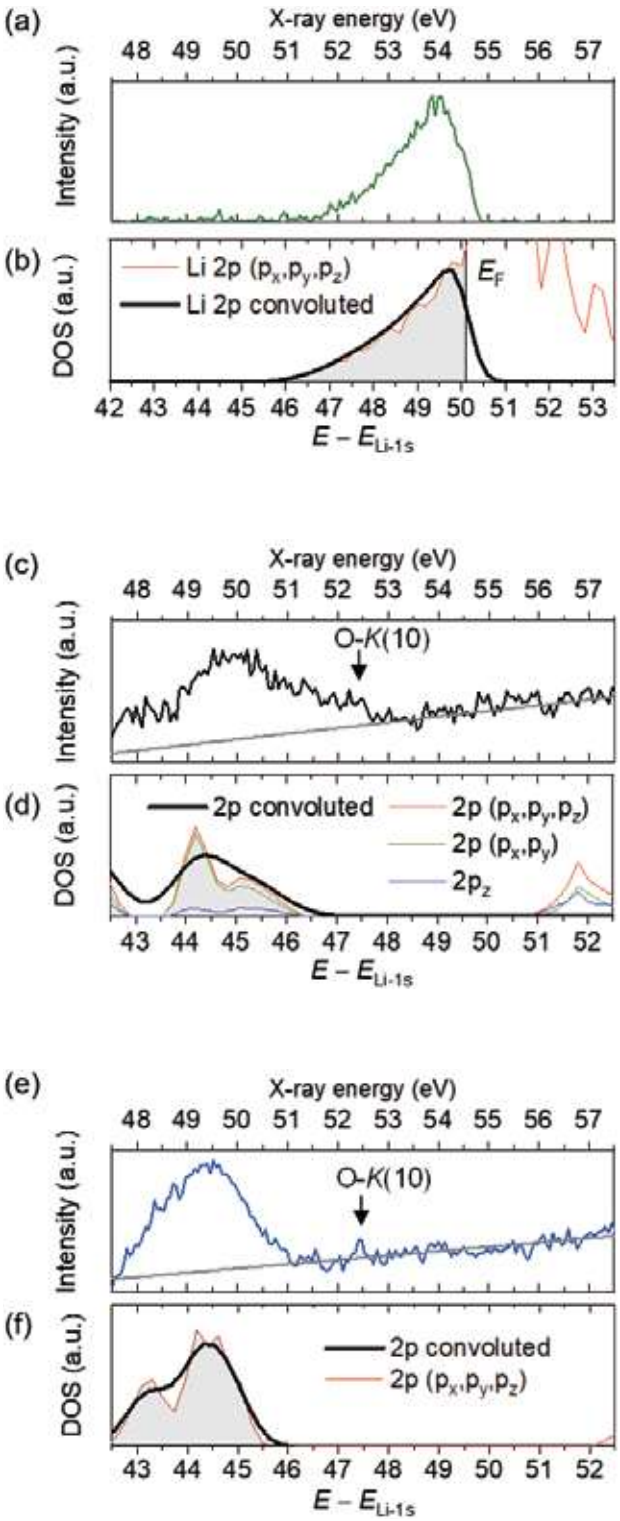

The Li–K spectra for Li (a), Li_2O_2(c), and Li_2O (e) using the SXES compared to the convoluted DOSs of occupied Li 2*p* states in Li metal (b), Li_2O_2(d), and Li_2O (f) using hybrid Heyd–Scuseria–Ernzerhof (HSE) functionals. Gray solid lines in panel (c) and (e) denotes linear background. Calculated energy is referenced to Li 1*s* centroid ($E_{\text{Li-1}s}$) where Li 2*p* occupied states below the Fermi energy are colored by gray.

poor signal to noise (S/N) ratios.

In **Fig. 2**, the SXES Li–K spectra are directly compared with the DOS of Li using the HSE functional. The energy was referenced to $E_{\text{Li-1s}}$. The calculated Li 2*p* occupied states were convoluted with Gaussian functions with full width at half-maxima (FWHM) of 0.6 eV (Li and Li_2O) and 0.9 eV (Li_2O_2) because of the difference in the calculated 1*s* band width. The shapes of Li–K spectra agreed well with the convoluted 2*p* occupied states. The calculated energies using HSE were underestimated as large as 4.0 eV for Li metal and 5.3 eV for the oxides. A comparison between the experimental spectra and DOS using PBE supports that the obtained spectral shapes describe Li valence electronic states, while the energetic underestimations were even larger with PBE.

The Li–K spectrum for Li_2O_2 mainly derived from antibonding π_g* orbitals appeared at 49–52 eV, while the peak of bonding orbitals (σg and π_u) were below the SXES low-energy limit. The contributions of both bonding and antibonding orbitals were seen in the broad peak of O–K(4) for Li_2O_2 in Fig. 1c. The O–K(4) FWHM of the Li_2O_2 sample was 2.26 times wider than that from the Li_2O sample, which was consistent with the valence band width ratio of 2.12 calculated using HSE. The wide valence band was attributed to the anisotropic 2*p* states in Li_2O_2. Although the unidentified O–*K* peak in Li_2O was observed at 528.9 eV in the previous SXES results [15], no peak was found at the corresponding position of 132.2 eV for O–K(4) in the Li_2O spectrum in the present work.

The chemical state and element mappings on a Li metal sample that has been naturally oxidized in air with a partial metallic surface are shown in **Fig. 3**. The SXES spectra were collected at 40 × 32 measuring points (1280 points), with an acquisition time of 30 s per pixel (pixel size: 1 μm × 1 μm).

Fig. 3

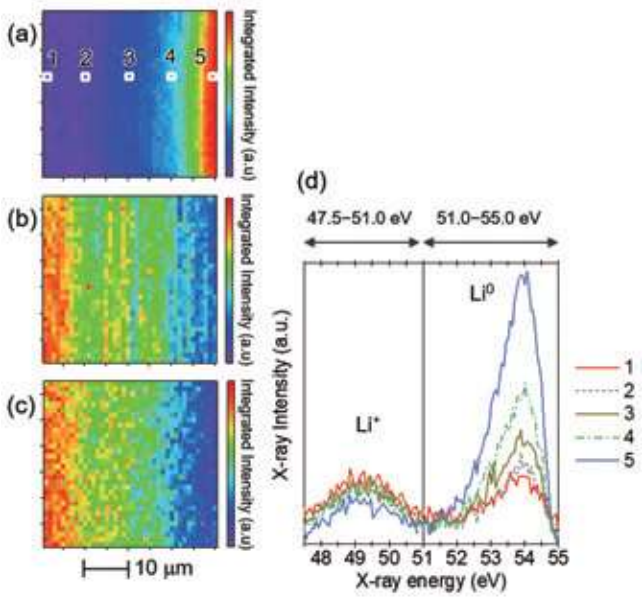

Chemical state mappings of Li metal (E = 51.0–55.0 eV) (a) and Li_2O (E = 47.5–51.0 eV) (b), element mapping of O using 4th order O–K (E = 129–132 eV) (c), and Li–K spectra at five measuring area (d). The positions of the five measuring area are shown in panel (a).

From the naturally oxidized Li metal sample, the Li–K spectra of Li_2O (E <51 eV) and Li (>51 eV) were observed without peak overlap. No Li_2O_2 peak was found from the collected data, as predicted by the MALT thermodynamic database. Figure 3 visualizes element and chemical state mappings in the naturally oxidized Li metal sample. The energy ranges for Li metal (Li^0) and Li_2O (Li^+) were set as 51.0–55.0 eV and 47.5–51.0 eV as shown in Fig. 3d. Chemical state mappings (Fig. 3a,b) visualize Li metal/oxide phase distribution on the sample; the metallic Li phase was distributed on the right side of the observed area, while the Li_2O phase lies on the left. Together with O element mapping (Fig. 3c), it is possible to distinguish the Li_2O phase from other oxide phases with lacking Li. Nevertheless, the visualization of oxide phases struggled with weak Li–K emissions from the oxide samples. For an identification whether Li_2O_2 or Li_2O phase in a Li–O_2 battery system, it is recommended to utilize O–K emissions rather than weak Li–K. A chemical state mapping of Li_2O_2 may be accomplished by integrating signals of the bonding orbitals appeared in the range of 128–130 eV for O–K(4) (Fig. 2c).

Analysis on Fe–Ti alloy immersed in liquid Li metal

Motivation

Liquid Li metal is a target material of an accelerator-based neutron source using d–Li stripping reaction [16]. N impurity is easily contained by liquid Li metal, which should be removed because it enhances corrosion of stainless tube [17]. As a trap material for removing N from liquid lithium metal, the use of Fe–Ti alloys has been proposed in order to overcome a low absorption rate of N by pure Ti [18]. However, distribution of trapped N within the Fe–Ti alloy have not been understood because characteristic X-ray emissions of N–Kα (392 eV) and Ti–Lℓ (395 eV) are close and thus highly overlapped with conventional devices such as EDX (energy dispersive X-ray spectrometer). Thus, by separating these peaks using the SXES with an ultra-high energy resolution, we investigated Ti and N distribution within the Fe–Ti alloy samples after immersing in liquid Li metal.

Experimental

Fe–Ti alloy spherical samples (diameter: 100–125 μm) containing 5 at.% of Ti were prepared by gas atomize method. 5.0 g of lithium (99.9% purity), Li_3N (99% purity) and 1.0 g of the alloys were enclosed in a SUS316L capsule in a glove box filled with Ar gas. Here, the amount of Li_3N was equal to 1000 wt.ppm of nitrogen concentration in liquid Li. The capsules were heated in an electric furnace for 9, 36, 81, and 256 h at 823 K. The SXES analysis was performed with the JS200N grating. The SXES spectra were collected by scanning the sample stage linearly in step of 1.0 μm from the surface toward the central part of the alloys. SXES analyses were performed with acceleration voltage of 15 kV, beam current of 120 nA, and exposure time of 1000 s. In order to separate second order peaks of N–Kα (392 eV) and Ti–Lℓ, reference energy spectra of nitrogen and titanium, f_N and f_{Ti}, were collected with ZrN powder (99% purity) and as-received Fe–Ti sample, respectively. The synthesized energy spectra f were obtained by fitting to the experimental spectra by the equation $f = k_N f_N + k_{Ti} f_{Ti}$ where k_N, k_{Ti}, f_N, and f_{Ti} are weighting coefficients of N and Ti, and reference spectra for N and Ti taken from ZrN and as-received Fe–Ti sample, respectively. In **Fig. 4**, as an example, the SXES spectrum from the Fe–Ti sample

immersed for 256 h and the synthesized spectrum are shown. Concentration of X (X = N, Ti, and Fe), C_X, was calculated as follows:

$$C_X = \int_{192}^{200} k_X f_X \mathrm{d}E$$

where is E is X-ray energy (eV).

Results and Discussion

Figure 5 shows the element mapping of Ti using Ti–Kα and the grain boundary distribution obtained from the cross section of the Fe–Ti sample immersed for 256 h in the liquid Li metal. From the overlaid image of EDX and electron backscattered diffraction (EBSD) in Fig. 5(c), high concentrations of Ti were seen in the grain boundaries. The XRD patterns from the immersed samples showed a gradual shift of diffraction peaks to higher 2θ angle as the immersion time became longer. This indicates a gradual decrease in interplanar spacing of α-Fe phase due to loss of dissolved titanium. Ti can exist a solute element in α-Fe phase up to the fraction of approximately 2 at.% at 823 K [19]. As the Fe–Ti sample was oversaturated state, dissolved Ti in the crystal grain was diffused during the immersion and finally trapped by segregated Ti in the grain boundaries.

The results of SXES line analysis in the immersed samples are shown in **Fig. 6**. The scan was carried out in the direction from the surface to the center of the samples. The immersed samples for 9–256 h had high N concentrations on the surfaces. In these samples, the peaks of Ti appeared with N peaks, indicating N impurities trapped at the grain boundaries. In the sample immersed for 256 h, the N peak was observed even in the central part of the spherical sample. This indicates that N diffusion and trapping is dominant on the surfaces and in the grain boundaries of the alloy samples. The concentration ratios of N/Ti were calculated by dividing C_N by C_{Ti}. The N/Ti ratio were independent on the immersion periods, where the ratios were high from the surfaces to 5 μm deep because of the surface trapping. It is indicated that nitrogen is trapped rapidly near the surface of alloy samples, and gradually trapped in the grain boundaries as nitrogen diffuses into the Fe–Ti alloy samples.

Mean N diffusivity in the Fe–Ti samples was estimated from the results of the SXES line analysis, in which the longest

Fig. 4

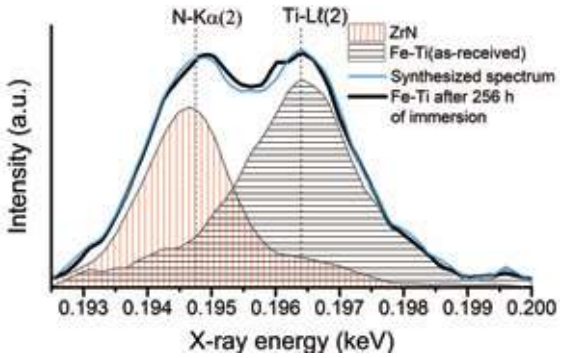

SXES spectrum from the Fe–Ti sample immersed in liquid Li metal for 256 h, synthesized spectrum, and reference spectra from ZrN and as-received Fe–Ti sample.

Fig. 5

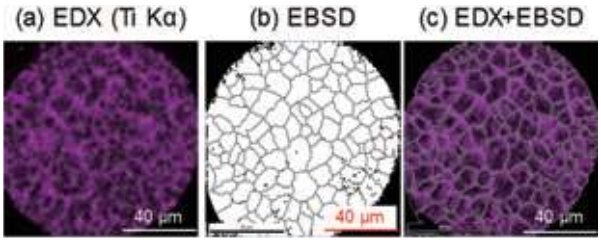

(a) Ti–K energy dispersive X-rays (EDX) mapping, (b) electron backscatter diffraction (EBSD) mapping, and (c) EDX + EBSD overlaid image of the Fe–Ti sample immersed for 256 h in the liquid Li metal.

Fig. 6

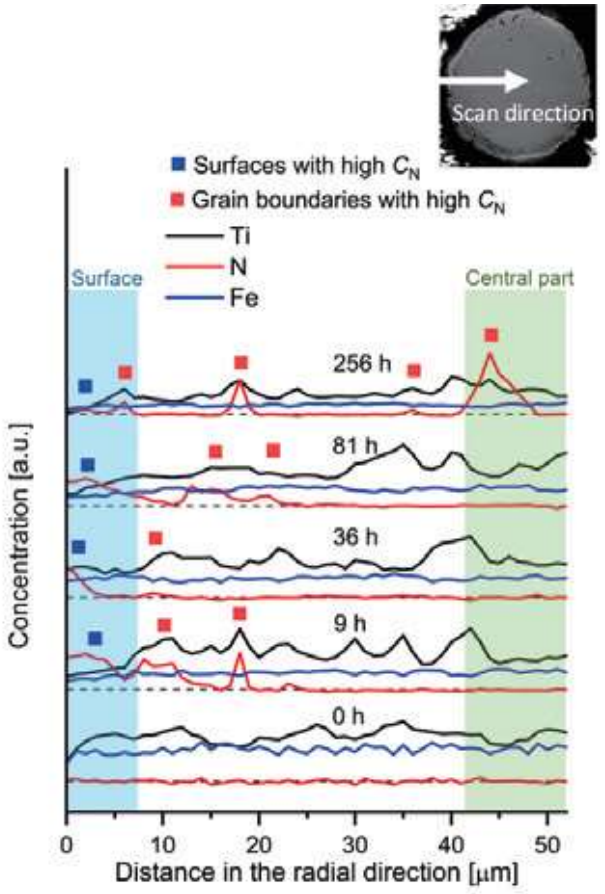

Concentrations of N, Ti, and Fe obtained by SXES line analysis for the cross sections of the Fe–Ti samples before and after immersion in the liquid Li metal. Inset SEM image shows the cross section, measurement positions, and scan direction.

distances of N peak from the surfaces were set as the mean diffusion distances. As a result, the N diffusivity in the Fe–Ti sample was estimated to be 5×10^{-16} m^2/s at 823 K. The obtained diffusivity was much higher than that in pure α–Ti (1.3×10^{-19} m^2/s) at 823 K [20]. It is considered that N diffuses in the Fe–Ti alloy much faster than that α–Ti because it diffuses through dominantly in α-Fe phase. The high N diffusivity of Fe–Ti alloy is a promising property as a getter material immersed in liquid Li metal.

Conclusion

In this study, electronic state analysis was carried out using the SXES for visualizing elemental and chemical state mappings. First, electronic states of Li metal and oxides were investigated and then compared with PDOS of Li using DFT calculations. Characteristic Li–Kα emissions from Li, Li_2O_2, and Li_2O were detected in the low energy region of 47.5–54.0 eV. By utilizing the Li 1*s* core-level shift in Li_2O, the chemical state mappings were successfully constructed. To overcome very weak signals of Li–K from Li oxides, it is proposed to set ROI in O–Kα emissions for visualizing Li_2O_2 and Li_2O phases separately. Second, the SXES peak analysis was carried out to separately visualize N and Ti distributions in the Fe–Ti alloy samples immersed in liquid Li metal. The results indicated that N is trapped rapidly near the surface of alloy samples, and gradually diffused along the grain boundaries. The mean diffusivity of N in the Fe–Ti samples was estimated to be 5×10^{-16} m^2/s from the results of the SXES line analysis.

Acknowledgments

This work is partially supported by the Joint Usage/Research Program on Zero-Emission Energy Research, Institute of Advanced Energy, Kyoto University (ZE29A-21, ZE30A-09). This work is also carried out with the support and under the auspices of the QST Collaborative Research Program. Prof. Satoshi Konishi (Kyoto University), Toshiro Sakabe (JSPS research fellowship DC2, Kyoto University), and Prof. Kazuya Sasaki (Hirosaki University) are thanked for helpful discussions.

References

[1] Terauchi, M.; Takahashi, H.; Handa, N.; Murano, T.; Koike, M.; Kawachi, T.; Imazono, T.; Koeda, M.; Nagano, T.; Sasai, H.; Oue, Y. Ultrasoft-X-ray emission spectroscopy using a newly designed wavelength-dispersive spectrometer attached to a transmission electron microscope. *J. Electron Microsc*. 2012, **61**, 1–8.

[2] Takahashi, H.; Murano, T.; Takakura, M.; Asahina, S.; Terauchi, M.; Koike, M.; Imazono, T.; Koeda, M.; Nagano, T. Development of soft X-ray emission spectrometer for EPMA/SEM and its application. *IOP Conf. Ser. Mater. Sci. Eng*. 2016, **109**, 012017.

[3] Kasada, R.; Mukai. K.; Chemical State Analysis of Light Elements in Nuclear Fission and Fusion Reactor Materials by Soft X-ray Emission Spectroscopy in Electron Probe Microanalyzer. *JEOL News* 2020, **55**, 32–35.

[4] Park, C.; Nozawa, T.; Kasada, R.; Tosti, S.; Konishi, S.; Tanigawa, H. The effect of wall flow velocity on compatibility of high-purity SiC materials with liquid Pb-Li alloy by rotating disc testing for 3000 h up to 900° C. *Fusion Eng. Des*. 2018, **136**, 623–627.

[5] Mukai, K.; Kasada, R.; Yabuuchi, K.; Konishi, S.; Kim, J.H.; Nakamichi, M. Valence Electron and Chemical State Analysis of $Be_{12}M$ (M = Ti, V) Beryllides by Soft X-ray Emission Spectroscopy. *ACS Appl. Energy Mater*. 2019, **2**, 2889–2895.

[6] Kasada, R.; Ha, Y.; Higuchi, T.; Sakamoto, K. Chemical State Mapping of Degraded B_4C Control Rod Investigated with Soft X-ray Emission Spectrometer in Electron Probe Micro-analysis. *Sci. Rep*. 2016, **6**(1), 1–6.

[7] Mukai, K.; Kasada, R.; Sasaki, K.; Konishi, S. Occupied Electronic States of Li in Li, Li_2O_2, and Li_2O Analyzed by Soft X-ray Emission Spectroscopy. *J. Phys. Chem. C* 2020, **124**, 9256–9260.

[8] Omura, R.; Yagi, J.; Mukai, K.; Oyaidzu, M.; Ochiai, K.; Kasugai, A.; Konishi, S. Analysis of nitrogen distribution in iron-titanium alloys after nitrogen trapping in liquid lithium by using soft X-ray emission spectroscopy, *Fusion Eng. Des*. 2021, **170**, 112548.

[9] Konishi, S.; Enoeda, M.; Nakamichi, M.; Hoshino, T.; Ying, A.; Sharafat, S.; Smolentsev, S. Functional materials for breeding blankets—status and developments. *Nucl. Fusion* 2017, **57**(9), 092014.

[10] Lai, J.; Xing, Y.; Chen, N.; Li, L.; Wu, F.; Chen, R. Electrolytes for rechargeable lithium–air batteries. *Angew. Chem. Int. Ed*. 2020, **59**(8), 2974–2997.

[11] Perdew, J.P.; Burke, K.; Ernzerhof, M. Generalized gradient approximation made simple. *Phys. Rev. Lett*. 1996, **77**, 3865–3868.

[12] Blöchl, P. E. Projector augmented-wave method. *Phys. Rev. B* 1994, **50**, 17953–17979.

[13] Kresse, G.; Furthmüller, J. Efficient iterative schemes for ab initio total-energy calculations using a plane-wave basis set. *Phys. Rev. B* 1996, **54**, 11169–11186.

[14] Heyd, J.; Scuseria, G.E.; Ernzerhof, M. Hybrid functionals based on a screened Coulomb potential. *J. Chem. Phys*. 2003, **118**, 8207–8215.

[15] Léon, A.; Fiedler, A.; Blum, M.; Benkert, A.; Meyer, F.; Yang, W.; Bär, M.; Scheiba, F.; Ehrenberg, H.; Weinhardt, L.; Heske, C. Valence Electronic Structure of Li_2O_2, Li_2O, Li_2CO_3, and LiOH Probed by Soft X-ray Emission Spectroscopy. *J. Phys. Chem. C* 2017, **121**, 5460–5466.

[16] Sato, S.; Kasugai, A.; Ochiai, K.; Masuda, K.; Nakamura, M.M.; Ohta, M.; Oyaidzu, M.; Kwon, S.; Sakamoto, K.; Ishida, S. Conceptual design of advanced fusion neutron source (A-FNS) and irradiation test modules. *Nucl. Fusion* 2021, **61**(10), 106026.

[17] Lyublinski, I.E.; Evtikhin, V.A.; Pankratov, V.Y.; Krasin, V.P. Numerical and experimental determination of metallic solubilities in liquid lithium, lithium-containing nonmetallic impurities, lead and lead-lithium eutectic. *J. Nucl. Mater*. 1995, **224**, 288–292.

[18] Hirakane, S.; Yoneoka, T.; Tanaka, S. Control of nitrogen concentration in liquid lithium by iron–titanium alloy, *Fusion Eng. Des*. 2006, **81**, 665–670.

[19] Bo H.; Wang J.; Duarte, L.; Leinenbach, C.; Liu, L.; Liu, H.; Jin, Z. Thermodynamic re-assessment of Fe–Ti binary system. Trans. *Nonferrous Met. Soc. China* 2012, **22**(9), 2204–2211.

[20] Metals Data Book, 4th ed., Japan Institutes of Metals, 1993.